# Chained LDPC Codes via Partial Information Coupling and Partial Parity Superposition

Qianfan Wang*, Li Chen†, and Xiao Ma‡
*School of Electronics and Communication Engineering, Sun Yat-sen University, Guangzhou 510006, China
†School of Electronics and Information Technology, Sun Yat-sen University, Guangzhou 510006, China
‡School of Computer Science and Engineering, Sun Yat-sen University, Guangzhou 510006, China
Email:wangqf6@mail2.sysu.edu.cn, {chenli55, maxiao}@mail.sysu.edu.cn

2021 IEEE Globecom Workshops (GC Wkshps) | 978-1-6654-2390-8/21/$31.00 ©2021 IEEE | DOI: 10.1109/GCWkshps52748.2021.9682151

***Abstract*—This paper presents a new class of chained low-density parity-check (LDPC) codes for the transport block (TB) based transmission protocol, in which a TB consists of multiple code blocks (CBs). The proposed chained LDPC codes are constructed by coupling together all CBs of a TB into a single chain, where partial information bits between every two adjacent LDPC CBs are shared using the partial information coupling (PIC) technique and partial parity bits are superimposed onto the following LDPC CB using the partial superposition (PS) technique, resulting in a PIC-PS-LDPC code. The proposed construction is *universal* in the sense that it is applicable to any existing LDPC codes including the random LDPC codes and the structured LDPC codes to obtain extra coding gains. More importantly, the proposed PIC-PS-LDPC codes can have encoder/decoder implemented using the structure of the underlying LDPC codes. Numerical results show that the PS technique can further improve the PIC-LDPC codes, and the PIC technique can further improve the PS-LDPC codes. They also show that the proposed PIC-PS-LDPC codes with the 5G New Radio (5G-NR) LDPC codes as the mother codes can yield a coding gain of up to $0.6$ dB over the conventional 5G-NR LDPC codes.**

***Index Terms*—5G New Radio (5G-NR), block Markov superposition transmission (BMST), low-density parity-check (LDPC) codes, partial superposition (PS), partial information coupling (PIC).**

## I. Introduction

Low-density parity-check (LDPC) codes were introduced by Gallager [1] and rediscovered by MacKay and Neal [2]. Recently, due to their good performance and high decoding throughput, the rate-compatible raptor-like LDPC codes have been adopted for data channels in 5G enhanced mobile broadband (eMBB) scenario [3].

In this work, we consider the design of LDPC codes for transport block (TB) based transmission, where a TB consists of multiple finite-length code blocks (CBs). Conventionally, each CB within one TB is separately encoded and decoded. This TB-based transmission is used for hybrid automatic repeat request (HARQ) protocol in both long-term evolution (LTE) [4] and 5G eMBB [5] standards for high speed data transmission. However, both TB-level HARQ retransmission in LTE and CB group (CBG)-level HARQ retransmission in 5G lead to a waste of transmission power and spectral efficiency since any erroneous CB will cause the retransmission of the whole TB or whole CBG. To improve the resource utilization efficiency of these protocols, one can improve the TB error rate (TBER) or CB error rate (CBER).

A well-known approach to improve the error-correction performance is spatial coupling. Typically, the spatially coupled LDPC (SC-LDPC) codes are constructed by coupling $L$ independent LDPC codes into a single chain [6, 7]. They can yield the asymptotically capacity-achieving performance over the binary-input memoryless symmetric (BMS) channels under the iterative belief propagation (BP) decoding [8]. This is due to the *threshold saturation*, where the BP decoding performance of the SC-LDPC codes can approach the maximum a posteriori (MAP) decoding performance of the underlying LDPC codes [7, 9]. Inspired by spatial coupling, the authors of [10, 11] proposed partial information coupling (PIC) technique to improve the performance, where a few information bits between the adjacent CBs are shared for encoding but transmitted only once by puncturing. Inspired by spatial coupling and block Markov superposition transmission (BMST) [12, 13], the authors of [14, 15] presented another spatial coupling approach via partial superposition (PS) to improve the performance, where a portion of the coded bits are selected and superimposed onto the following codewords.

An interesting question arises that the aforementioned two techniques can be integrated to obtain extra coding gains. To this end, we present for the TB-based transmission a new class of chained LDPC codes, referred to as PIC-PS-LDPC codes. The PIC-PS-LDPC codes are constructed by coupling together $L$ LDPC CBs into a single chain, in which the information bits are coupled by the PIC technique and the parity bits are coupled by the PS technique. The construction of the PIC-PS-LDPC codes is universal since it is applicable to any existing LDPC codes, e.g., the 5G New Radio (5G-NR) LDPC codes to obtain extra coding gains. In addition, the PIC-PS-LDPC codes can be easily implemented with the hardware structure of the underlying LDPC codes. The PIC-LDPC codes and the PS-LDPC codes can be viewed as subclasses of the PIC-PS-LDPC codes with special parameters. Consequently, by optimizing the parameters, one can expect extra coding gains. In simulation, we employ the $(3,\ 6)$-regular LDPC codes, the WiMAX LDPC codes and the 5G-NR LDPC codes as the mother codes to construct the PIC-PS-LDPC

This work was supported by the National Key R&D Program of China (No. 2020YFB1807100), the NSF of China (No. 61971454 and No. 62071498) and the Key-Area Research and Development Program of Guangdong Province (No. 2018B010114001). *(Corresponding author: Xiao Ma.)*

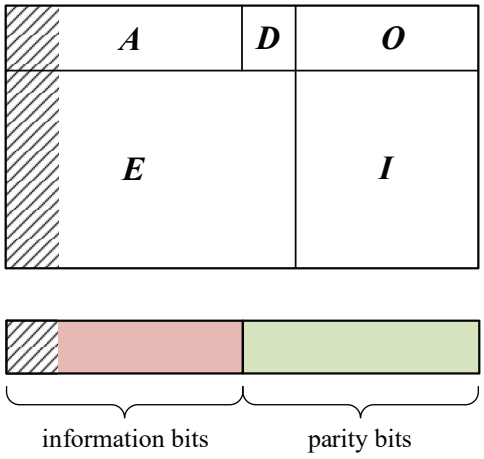


Fig. 1. An illustration of the parity-check matrix and the corresponding codeword for the 5G-NR LDPC code.

codes. The simulation results show that the PS technique can further improve the PIC-LDPC codes and the PIC technique can further improve the PS-LDPC codes. They also show that the PIC-PS-LDPC codes can yield an extra coding gain of up to 0.6 dB over the 5G-NR LDPC codes.

## II. Preliminaries

### A. 5G-NR LDPC Codes

The 5G-NR LDPC code is a class of rate-compatible LDPC codes with raptor-like quasi-cyclic (QC) construction. Two base matrices (equivalently, two base graphs BG1 and BG2), which encapsulate the desired macroscopic structure, have been designed for different range of information lengths and code rates [5]. A specific NR LDPC code can be defined by a parity-check matrix constructed by lifting the base matrix with a lifting factor $Z$. The structure diagram of the parity-check matrix and the corresponding codeword of the NR LDPC code are illustrated in Fig. 1, where $\boldsymbol{A}$ and $\boldsymbol{E}$ consist of circulant permutation matrices and zero matrices, $\boldsymbol{D}$ is a dual-diagonal matrix with the exception that its first column has weight of three, $\boldsymbol{I}$ is an identity matrix and $\boldsymbol{O}$ is a zero matrix. Part $\boldsymbol{A}$ corresponds to the systematic information bits, while part $\boldsymbol{D}$ and part $\boldsymbol{I}$ correspond to the parity bits.

### B. Partial Information Coupling

The PIC technique was first introduced in [10] to construct the PIC-turbo codes by sharing a portion of information bits between the adjacent CBs, where the portion is characterized by a parameter called coupling fraction $\beta$, $0 \leqslant \beta \leqslant 0.5$. The PIC-turbo codes can achieve considerable coding gains over the LTE turbo codes. Using the IEEE 802.16e (WiMAX) LDPC codes as the mother codes, the PIC-LDPC codes were presented in [11], which can yield a coding gain of more than 0.5 dB over the WiMAX LDPC codes. In the PIC technique, the dummy bits, which are inserted at the first and last CBs, can provide extra a priori information to the decoder of the mother code and hence improve performance of these two CBs. Due to the shared information bits between the adjacent

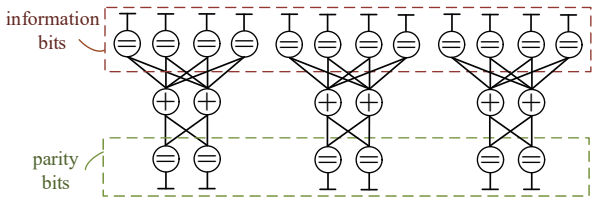


(a) The normal graph of three (2, 6)-regular LDPC codes with length 6.

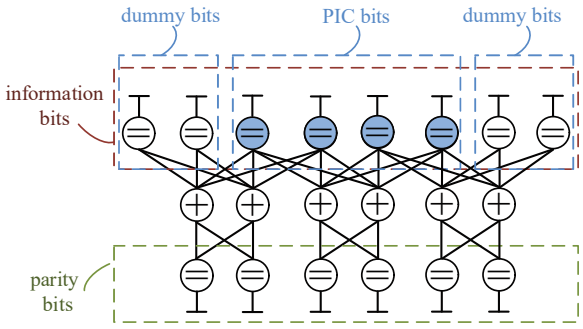


(b) The normal graph of the PIC-LDPC codes.

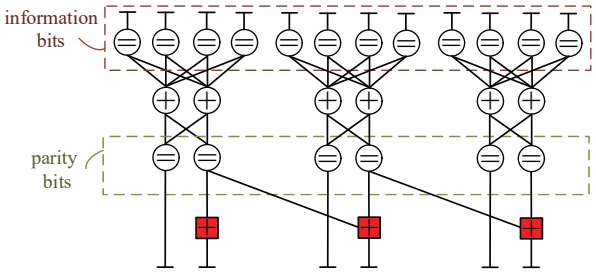


(c) The normal graph of the PS-LDPC codes.

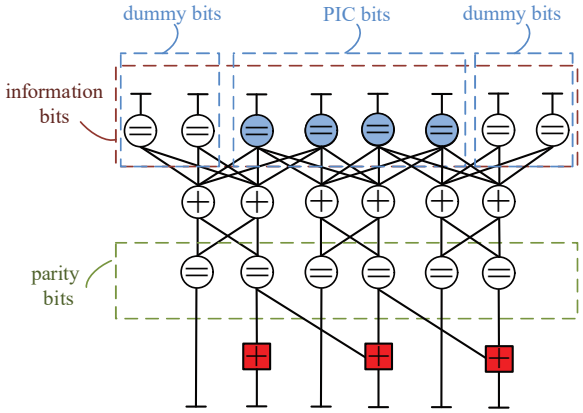


(d) The normal graph of the PIC-PS-LDPC codes.

Fig. 2. The normal graph of the (2, 6)-regular LDPC codes with length 6, the PIC-LDPC codes, the PS-LDPC codes and the PIC-PS-LDPC codes, where the up variable nodes correspond to the information bits, the down variable nodes correspond to the parity bits, the blue variable nodes correspond to the PIC bits, the circular check nodes correspond to the LDPC check nodes, and the red square nodes correspond to the PS bits. Notice that the LDPC check nodes and the red PS nodes have the same constraint that all connecting variables must be added up to zero over $\mathbb{F}_2$.

CBs, the reliable messages can be spread from the CBs at the boundary of the chain to other CBs, and hence, the error-correction performance can be improved.

Given a binary code of length $n$ and dimension $k$, the real code rate of the PIC code with dummy bits is given by

$$r_r = \frac{L(k - \lfloor \beta k \rfloor) - \lfloor \beta k \rfloor}{L(n - \lfloor \beta k \rfloor) - \lfloor \beta k \rfloor}, \tag{1}$$

where $L$ denotes the coupling length and $\lfloor\ \rfloor$ denotes the floor function. We present a simple example with the (2, 6)-regular LDPC code to illustrate the PIC technique. Fig. 2(a) shows the normal graph of the (2, 6)-regular LDPC codes, and Fig. 2(b) shows the corresponding PIC-LDPC codes, where the coupling fraction is $\beta = 0.5$.

### C. Partial Superposition

The PS technique enables a portion bits of the previous LDPC codeword to be superimposed (XORed) onto the current LDPC codeword [14, 15], where the portion is characterized by a parameter called superposition fraction $\alpha$, $0 \leqslant \alpha \leqslant 1$. With the random LDPC codes as the basic codes, the PS-LDPC codes (referred to as BMST-LDPC codes in [15]) can yield a coding gain of up to 1.0 dB over the underlying LDPC codes. In this paper, the PS technique is only used for the parity bits and $\alpha$ is the parity superposition fraction. With the (2, 6)-regular LDPC codes as the mother codes, the PS-LDPC codes are shown in Fig. 2(c), where the parity superposition fraction is $\alpha = 0.5$.

## III. PIC-PS-LDPC Codes

The PIC-PS-LDPC codes are constructed by coupling the information bits between the adjacent CBs using the PIC technique and by coupling the parity bits between the adjacent CBs using the PS technique. With the (2, 6)-regular LDPC codes as the mother codes, the normal graph of the PIC-PS-LDPC codes is shown in Fig. 2(d), where $\alpha = 0.5$ and $\beta = 0.5$. Notice that $\alpha$ and $\beta$ are the key parameters of the PIC-PS-LDPC codes and can be optimized numerically by two-dimensional search. Also notice that the PIC-PS-LDPC codes is reduced to the PIC-LDPC codes when $\alpha = 0$, and the PIC-PS-LDPC codes is reduced to the PS-LDPC codes when $\beta = 0$. In other words, the PIC-PS-LDPC codes include the PIC-LDPC codes and the PS-LDPC codes as sub-classes.

### A. Encoder

Let $\mathscr{C}[n, k]$ denote a systematic binary LDPC code with length $n$ and dimension $k$, whose parity-check matrix is denoted by $\mathbf{H}$. The information sequence to be transmitted for a TB of $L$ CBs is written as $\boldsymbol{u} = (\boldsymbol{u}_1, \boldsymbol{u}_1^c, \boldsymbol{u}_2, \boldsymbol{u}_2^c, \cdots, \boldsymbol{u}_{L-1}, \boldsymbol{u}_{L-1}^c, \boldsymbol{u}_L)$, where the length of each uncoupled block $\boldsymbol{u}_\ell$ is $k' = k - 2\lfloor \beta k \rfloor$ and that of each coupled block $\boldsymbol{u}_\ell^c$ is $k_c = \lfloor \beta k \rfloor$. Let $\boldsymbol{u}_0^c \in \mathbb{F}_2^{k_c}$ and $\boldsymbol{u}_L^c \in \mathbb{F}_2^{k_c}$ denote the two dummy blocks, which are used for the first and the last CBs, respectively. For the PS technique with a parity superposition fraction $\alpha$, we define a *parity selection matrix* $\mathbf{S}$, which is confined to have the following form

$$\mathbf{S} = \begin{bmatrix} \mathbf{O} & \\ & \mathbf{I} \end{bmatrix}, \tag{2}$$

where $\mathbf{I}$ is an identity sub-matrix of order $\lfloor \alpha(n-k) \rfloor$ and $\mathbf{O}$ is a zero matrix of order $n - k - \lfloor \alpha(n-k) \rfloor$. Given the aforementioned uncoupled blocks, coupled blocks and two dummy blocks, the encoding algorithm of the PIC-PS-LDPC codes is described in Algorithm 1, see Fig. 3 for reference.

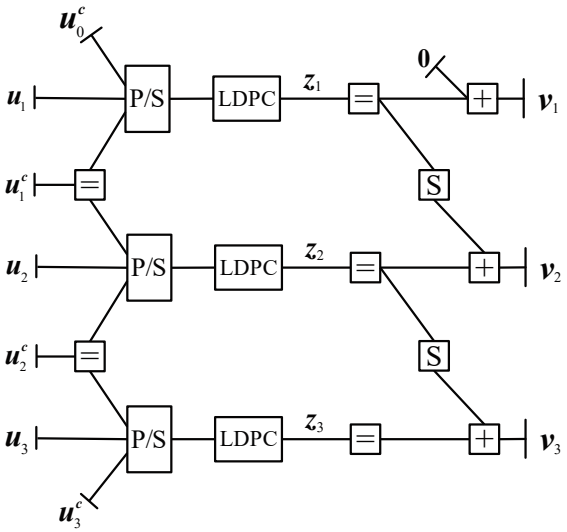


Fig. 3. The high-level normal graph of a PIC-PS-LDPC code with $L = 3$, where $\boldsymbol{u}_0^c$ and $\boldsymbol{u}_3^c$ denote the two dummy blocks.

**Algorithm 1** Encoding of the PIC-PS-LDPC Codes for a TB

- **Initialization**: Set $\boldsymbol{u}_0^c = \mathbf{0} \in \mathbb{F}_2^{k_c}$ and $\boldsymbol{z}_0 = \mathbf{0} \in \mathbb{F}_2^{n-k}$.
- **Recursion**: For $\ell = 1, 2, \cdots, L-1$,
  1) Take $(\boldsymbol{u}_{\ell-1}^c, \boldsymbol{u}_\ell, \boldsymbol{u}_\ell^c)$ as the input for the systematic LDPC CB encoder and deliver the parity bits $\boldsymbol{z}_\ell$ as the output.
  2) Compute the superposition parity bits $\boldsymbol{v}_\ell = \boldsymbol{z}_\ell + \boldsymbol{z}_{\ell-1}\mathbf{S}$, where $\mathbf{S}$ is a parity selection matrix.
  3) Arrange $\boldsymbol{c}_\ell = (\boldsymbol{u}_\ell, \boldsymbol{u}_\ell^c, \boldsymbol{v}_\ell)$ by juxtaposition, which is taken as the $\ell$-th coded block.
- **Termination**: The $L$-th coded block for transmission is obtained with Step **Recursion** by setting $\boldsymbol{u}_L^c = \mathbf{0}$. In particular, the $L$-th coded block is $\boldsymbol{c}_L = (\boldsymbol{u}_L, \boldsymbol{v}_L)$, where $\boldsymbol{u}_L^c$ is punctured[1].

### B. Decoder

Assume that a TB $\boldsymbol{c} = (\boldsymbol{c}_1, \boldsymbol{c}_2, \cdots, \boldsymbol{c}_L)$ is transmitted though a channel, resulting in a received vector $\boldsymbol{y} = (\boldsymbol{y}_1, \boldsymbol{y}_2, \cdots, \boldsymbol{y}_L)$ at the receiver. We can compute from the received vector $\boldsymbol{y}$ the log-likelihood ratios (LLRs) associated with $\boldsymbol{c}$ as the input to the decoding algorithm. The PIC-PS-LDPC codes can be decoded by the iterative sliding-window (SW) decoding algorithm, which can be described as

[1]Due to the two dummy blocks, the code length is $L(n - \lfloor \beta k \rfloor) - \lfloor \beta k \rfloor$ and the real code rate is $r_r = \frac{L(k-\lfloor \beta k \rfloor) - \lfloor \beta k \rfloor}{L(n-\lfloor \beta k \rfloor) - \lfloor \beta k \rfloor} \approx \frac{k - \lfloor \beta k \rfloor}{n - \lfloor \beta k \rfloor}$ for $L \gg 1$.

a message-passing algorithm over a high-level normal graph containing $d$ (the window size) layers, see Fig. 3 for reference. Each decoding layer consists of a node of type $\boxed{+}$, a node of type $\boxed{\mathbf{S}}$, two nodes of type $\boxed{=}$, a node of type $\boxed{\text{LDPC}}$, and a node of type $\boxed{\text{P/S}}$. The message-updating rules of these nodes are outlined below, see [16] for details.

- **Node** $\boxed{+}$: The node $\boxed{+}$ corresponds to the parity bits in this paper. The message-updating rule of this node is similar to that of the check node in an LDPC code, where the difference is that the messages associated with the half edges are computed from the channel observations.
- **Node** $\boxed{\text{S}}$: The node $\boxed{\text{S}}$ represents the parity selection matrix, which simply transfers the messages associated with the selected bits and the superimposed bits between the node $\boxed{=}$ and the node $\boxed{+}$.
- **Node** $\boxed{=}$: The node $\boxed{=}$ at the left of the normal graph corresponds to the information bits in this paper. The message-updating rule of this node is similar to that of the variable node in an LDPC code, where the difference is that the messages associated with the half edges are computed from the channel observations.
- **Node** $\boxed{\text{LDPC}}$: The message updating of the node $\boxed{\text{LDPC}}$ is implemented based on a certain soft-input soft-output (SISO) decoder, say, the sum-product algorithm (SPA) with a maximum iteration number $I_{\max}$, of the LDPC codes.
- **Node** $\boxed{\text{P/S}}$: The node $\boxed{\text{P/S}}$ represents a parallel-to-serial converter from the information bits to the node $\boxed{\text{LDPC}}$ and a serial-to-parallel converter for the opposite direction.

The SW decoding algorithm for the PIC-PS-LDPC codes is outlined in Algorithm 2. Notice that the messages associated with the half edges of the high-level normal graph are calculated from the channel observations for the transmitted bits or set properly as a fixed value for the dummy bits. Of course, the decoding algorithm can also be performed for the whole TB (referred to as a TB decoding algorithm in [11]), where all $\hat{\boldsymbol{u}}$ is output until all CBs are decoded successfully or a preset maximum number of global iterations is reached.

It should be pointed out that the proposed PIC-PS-LDPC codes with the SW decoding algorithm, especially the TB decoding algorithm, will increase the decoding latency. However, in terms of the total end-to-end latency, the latency for retransmission (order of multiple milliseconds) is much larger than the decoding latency. In the moderate-to-high SNR region, the PIC-PS-LDPC codes under the proposed decoding algorithms yield a much lower TBER or CBER than the benchmark LDPC codes without chaining. This leads to a much lower retransmission probability and hence a potential lower total end-to-end transmission latency.

**Algorithm 2** Iterative Sliding-Window Decoding Algorithm of the PIC-PS-LDPC Codes (window size $d \geq 1$)

- **Global initialization**: Set a maximum global iteration number $J_{\max} > 0$. For $1 \leq \ell \leq d-1$, compute the LLRs associated with $\boldsymbol{c}_\ell$ from the received vector $\boldsymbol{y}_\ell$. Since $\boldsymbol{u}_0^c = \boldsymbol{u}_L^c = \mathbf{0}$ is considered in this paper and the dummy bits are known by the decoder in advance, the LLRs associated with the dummy bits are set as $\infty$. All messages over the other edges within and connecting to the $\ell$-th layer $(1 \leq \ell \leq d-1)$ are initialized as uniformly distributed variables.
- **Sliding-window decoding**: For $\ell = 1, 2, \cdots, L$,
  1) ***Local initialization***: If $\ell + d \leq L$, compute the LLRs from the received vector $\boldsymbol{y}_{\ell+d}$ and all messages over other edges within and connecting to the $(\ell+d)$-th layer are initialized as uniformly distributed variables.
  2) ***Iteration***: For $j = 1, 2, \cdots, J_{\max}$,
     a) *Forward recursion*: For $i = 1, 2, \cdots, d$, the $(\ell + i)$-th layer performs a message-passing algorithm scheduled as
     $$\boxed{+} \rightarrow \boxed{=} \rightarrow \boxed{\text{LDPC}} \rightarrow \boxed{\text{P/S}} \rightarrow \boxed{=} \rightarrow \boxed{\mathbf{S}}.$$
     b) *Backward recursion*: For $i = d, d-1, \cdots, 1$, the $(\ell + i)$-th layer performs a message-passing algorithm scheduled as
     $$\boxed{=} \rightarrow \boxed{\text{LDPC}} \rightarrow \boxed{\text{P/S}} \rightarrow \boxed{=} \rightarrow \boxed{+} \rightarrow \boxed{\mathbf{S}}.$$
     c) *Decisions*: Make decisions on the LDPC codeword $\boldsymbol{w}_\ell = (\boldsymbol{u}_{\ell-1}^c, \boldsymbol{u}_\ell, \boldsymbol{u}_\ell^c, \boldsymbol{z}_\ell)$, resulting in $\hat{\boldsymbol{w}}_\ell$. If $\mathbf{H}\hat{\boldsymbol{w}}_\ell^{\mathrm{T}} = 0$, exit the iteration. Notice that the parity-check stopping criterion is also used in the above ***Iteration***, where the node $\boxed{\text{LDPC}}$ performs an iterative BP with a preset maximum iteration number $I_{\max}$.
  3) ***Successive cancellation***: Output $(\hat{\boldsymbol{u}}_\ell, \hat{\boldsymbol{u}}_\ell^c)$ if $\ell < L$ or $\hat{\boldsymbol{u}}_\ell$ if $\ell = L$ based on $\hat{\boldsymbol{w}}_\ell$ and remove the effect of $\hat{\boldsymbol{z}}_\ell$ on $\boldsymbol{y}_{\ell+1}$.

## IV. Simulation Results

In this section, we present the simulation results of the PIC-PS-LDPC codes. We use the (3, 6)-regular LDPC codes constructed by the PEG algorithm [17], the WiMAX LDPC codes and the 5G-NR LDPC codes as the mother codes. Unless otherwise stated, for the PIC-PS-LDPC codes, a TB consists of $L = 40$ CBs. The SW decoding algorithm (Algorithm 2) or the TB decoding algorithm is employed for the decoding. Unless otherwise stated, the maximum SPA iteration number is 100 for independent LDPC codes. In all example, the TB codewords $\boldsymbol{c}$ are transmitted over the AWGN channel with BPSK modulation.

*Example 1* (PIC-PS-LDPC Code with Random LDPC Code): Consider a rate-$1/2$ (3, 6)-regular LDPC code with length $1024$ as the mother code. The decoding window size of the chained codes is $d = 3$, where $J_{\max} = 20$ and $I_{\max} = 25$. The CBER performance with different $\alpha$ is shown in Fig. 4(a), where we observe that the PIC-PS-LDPC codes with properly selected $\alpha$ can outperform the PIC-LDPC codes (yielding a coding gain of up to 0.4 dB at $\mathrm{CBER} = 10^{-3}$), suggesting that the PS technique can further improve performance of the PIC-LDPC codes. The CBER performance with different $\beta$ is shown in Fig. 4(b), where we observe that the PIC-PS-LDPC codes with properly selected $\beta$ can outperform the

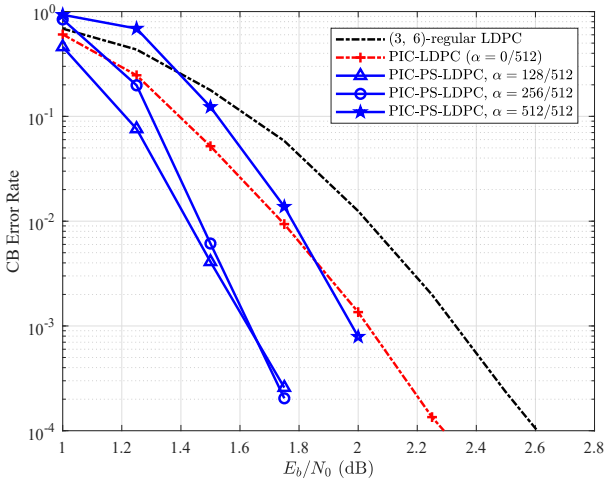


(a) Varying $\alpha$, fixed $\beta = 64/512$.

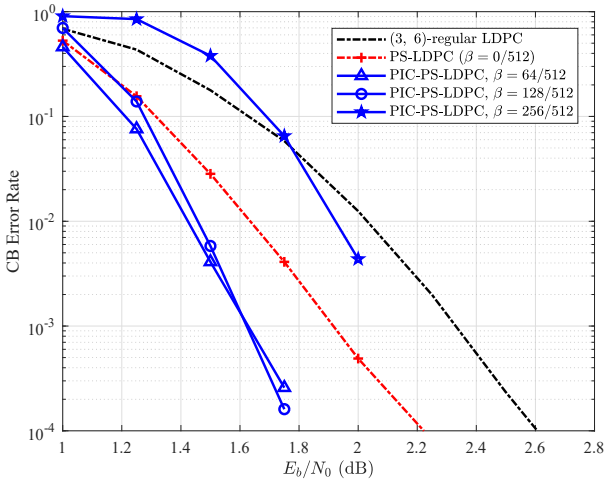


(b) Varying $\beta$, fixed $\alpha = 128/512$.

Fig. 4. The CBER performance of the PIC-PS-LDPC code, the PIC-LDPC code, the PS-LDPC code and the LDPC code. The mother code is a rate-1/2 $(3,\ 6)$-regular LDPC code of length 1024 and the decoding window size is $d = 3$.

PS-LDPC codes (yielding a coding gain of up to 0.3 dB at $\text{CBER} = 10^{-3}$), suggesting that the PIC technique can further improve performance of the PS-LDPC codes.

*Example 2* (PIC-PS-LDPC Code with WiMAX LDPC Code): The mother code is a rate-$2/3$-A WiMAX LDPC code with a length of 576 bits, which is constructed by lifting the base matrix with a lifting factor of $Z = 24$. For the PIC-PS-LDPC code, we set $\alpha = 24/192$ and $\beta = 180/384$. We also present performance of the PIC-LDPC code proposed in [11] and the rate-$1/2$ WiMAX LDPC codes of length 384, both of which have a similar code rate and TB length. The TB decoding algorithm is performed for the PIC-PS-LDPC code and the PIC-LDPC code, where $J_{\max} = 20$ and $I_{\max} = 200$. The TBER performance comparison is shown in Fig. 5, where we observe that the PIC-PS-LDPC code can perform as well as (or slightly better than) the PIC-LDPC code [11] in the waterfall region but with a higher real code rate due to the

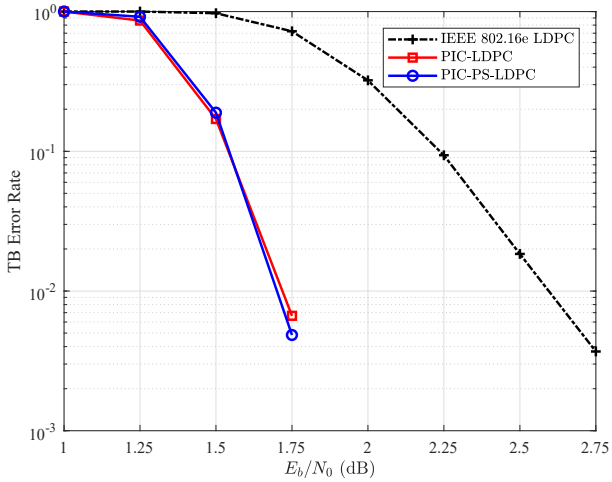


Fig. 5. The mother code is an IEEE 802.16e rate-$2/3$-A LDPC code with a length of 576 bits and the TB decoding algorithm is performed for the decoding. Similar to [11], we set $J_{\max} = 20$ and $I_{\max} = 200$, while the independent LDPC code is decoded with a maximum iteration number of 200. A TB of the PIC-PS-LDPC code and the PS-LDPC code consists of 45 CBs and that of the WiMAX LDPC code consists of 30 CBs, resulting in a similar TB length. The real code rates of the PIC-PS-LDPC code, the PIC-LDPC codes and the WiMAX LDPC code are 0.5102, 0.4944 and 0.5, respectively.

different coupling fraction $\beta$. We also observe that the PIC-PS-LDPC code can yield a coding gain of up to 0.9 dB over the WiMAX LDPC code, at the TBER of $10^{-2}$.

*Example 3* (PIC-PS-LDPC Code with 5G-NR LDPC Code): The mother code is a rate-1/2 5G-NR LDPC code of length 1280 bits, which is constructed based on BG2 [5] with a lifting factor $Z = 64$. For the PIC-PS-LDPC code, we set $\alpha = 384/768$ and $\beta = 64/640$, while for the PIC-LDPC code, we set $\alpha = 0/768$ and $\beta = 64/640$. To make a fair comparison, we also present a benchmark 5G-NR LDPC code with a similar code rate and CB length. The TB decoding algorithm is employed with $J_{\max} = 20$ and $I_{\max} = 50$. The CBER performance comparison is shown in Fig. 6(a), where we observe that the PIC-PS-LDPC code can outperform the PIC-LDPC code and the 5G-NR LDPC code, yielding a 0.4 dB coding gain over the PIC-LDPC code and a 0.6 dB coding gain over the 5G-NR LDPC code, at the CBER of $10^{-4}$.

We also compare the decoding convergence in terms of average number of iterations for performing the LDPC CB decoder for each TB, as shown in Fig. 6(b). From this figure, we can observe that the PIC-PS-LDPC code exhibits a higher decoding iteration number when the SNR is low. However, as the SNR increases, this number will converge to that of the benchmark LDPC code. That is, the complexity of the PIC-PS-LDPC code will be close to that of the LDPC code in the high SNR region.

## V. Conclusions

This paper has presented a new class of chained LDPC codes for the TB-based transmission, in which all CBs of a TB are coupled into a single chain by using the PIC technique and the PS technique. The construction of the proposed codes is universal in the sense that any existing LDPC codes can

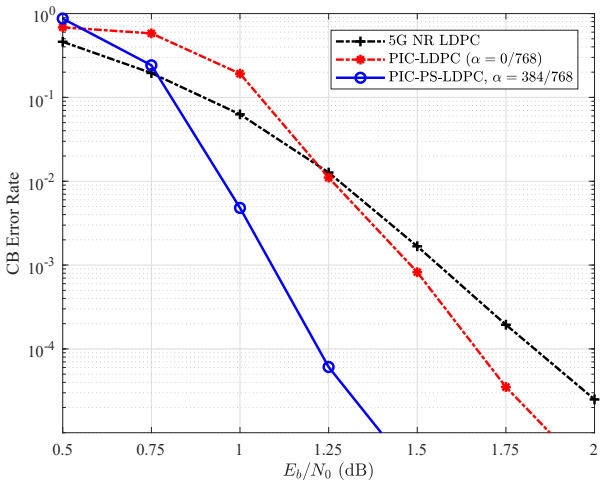


(a) The CBER performance.

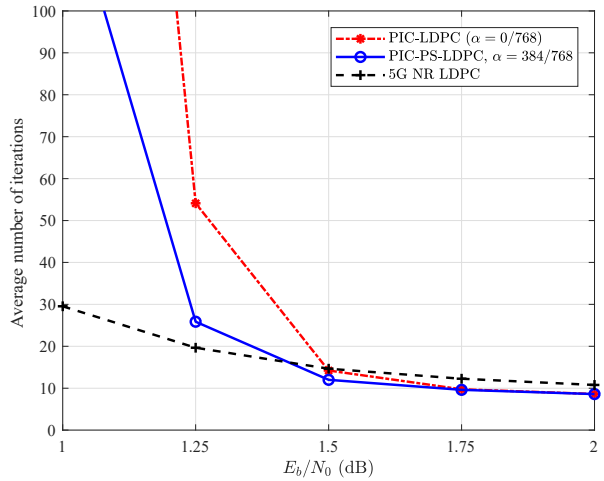


(b) The decoding convergence in terms of the average number of iterations for performing the LDPC CB decoder.

Fig. 6. The CBER performance and the decoding convergence of the PIC-PS-LDPC code, the PIC-LDPC code and the 5G-NR LDPC code. The mother code is a rate-1/2 5G-NR LDPC code of length 1280 bits and the benchmark LDPC code is a 5G-NR LDPC code with length 1216 and dimension 576. The real code rates of the PIC-PS-LDPC code, the PIC-LDPC code and the 5G-NR LDPC code are 0.4730, 0.4730 and 0.4737, respectively.

be used to construct the PIC-PS-LDPC codes. Moreover, the proposed PIC-PS-LDPC codes can be implemented with the hardware basis of the underlying LDPC codes. Our simulation results have shown that the PS technique can improve the PIC-LDPC codes and the PIC technique can improve the PS-LDPC codes. They have also shown that the proposed PIC-PS-LDPC codes can have an extra coding gain of up to 0.6 dB over the original 5G-NR LDPC codes.

## ACKNOWLEDGMENT

The first author would like to thank Dr. Suihua Cai for his helpful discussions.

## REFERENCES

[1] R. Gallager, "Low-density parity-check codes," *IRE Trans. Inf. Theory*, vol. 8, no. 1, pp. 21–28, Jan. 1962.
[2] D. J. C. MacKay and R. M. Neal, "Near Shannon limit performance of low density parity check codes," *Electron. Lett.*, vol. 32, no. 18, pp. 1645–1646, Aug. 1996.
[3] 3GPP, Final report of 3GPP TSG RAN WG1 #87 v1.0.0, 3GPP, Tech. Rep., Feb. 2017.
[4] LTE, Evolved Universal Terrestrial Radio Access, Physical Layer Procedures, Release 13, document, 3GPP TS 36.213, May 2016.
[5] 3GPP, Multiplexing and channel coding (Release 15), 3GPP TS 38.212 V15.1.1, Apr. 2018.
[6] A. J. Felstrom and K. S. Zigangirov, "Time-varying periodic convolutional codes with low-density parity-check matrix," *IEEE Trans. Inf. Theory*, vol. 45, no. 6, pp. 2181–2191, Sep. 1999.
[7] S. Kudekar, T. Richardson, and R. Urbanke, "Threshold saturation via spatial coupling: Why convolutional LDPC ensembles perform so well over the BEC," *IEEE Trans. Inf. Theory*, vol. 57, no. 2, pp. 803–834, Feb. 2011.
[8] ——, "Spatially coupled ensembles universally achieve capacity under belief propagation," *IEEE Trans. Inf. Theory*, vol. 59, no. 12, pp. 7761–7813, Dec. 2013.
[9] M. Lentmaier, A. Sridharan, D. J. Costello, and K. S. Zigangirov, "Iterative decoding threshold analysis for LDPC convolutional codes," *IEEE Trans. Inf. Theory*, vol. 56, no. 10, pp. 5274–5289, Oct. 2010.
[10] L. Yang, Y. Xie, X. Wu, J. Yuan, X. Cheng, and L. Wan, "Partially information-coupled turbo codes for LTE systems," *IEEE Trans. Commun.*, vol. 66, no. 10, pp. 4381–4392, Oct. 2018.
[11] L. Yang, Y. Xie, J. Yuan, X. Cheng, and L. Wan, "Chained LDPC codes for future communication systems," *IEEE Commun. Lett.*, vol. 22, no. 5, pp. 898–901, May 2018.
[12] C. Liang, X. Ma, Q. Zhuang, and B. Bai, "Spatial coupling of generator matrices: A general approach to design good codes at a target BER," *IEEE Trans. Commun.*, vol. 62, no. 12, pp. 4211–4219, Dec. 2014.
[13] X. Ma, C. Liang, K. Huang, and Q. Zhuang, "Block Markov superposition transmission: Construction of big convolutional codes from short codes," *IEEE Trans. Inf. Theory*, vol. 61, no. 6, pp. 3150–3163, Jun. 2015.
[14] Q. Wang, S. Cai, L. Chen, and X. Ma, "A throughput-enhanced HARQ scheme for 5G system via partial superposition," *IEEE Commun. Lett.*, vol. 24, no. 10, pp. 2162–2166, Oct. 2020.
[15] Q. Wang, S. Cai, W. Lin, S. Zhao, L. Chen, and X. Ma, "Spatially coupled LDPC codes via partial superposition and their application to HARQ," *IEEE Trans. Veh. Technol.*, vol. 70, no. 4, pp. 3493–3504, Apr. 2021.
[16] Q. Wang, S. Cai, W. Lin, L. Chen, and X. Ma, "Spatially coupled LDPC codes via partial superposition," in *IEEE Int. Symp. Inf. Theory*, Paris, France, July 2019, pp. 2614–2618.
[17] Xiao-Yu Hu, E. Eleftheriou, and D. M. Arnold, "Regular and irregular progressive edge-growth Tanner graphs," *IEEE Trans. Inf. Theory*, vol. 51, no. 1, pp. 386–398, Jan. 2005.